Inorg. Chem. **2005**, *44*, 5798–5804

Self-Assembly of Heterobimetallic Neutral Macrocycles Incorporating Ferrocene Spacer Groups: Spectroelectrochemical Analysis of the Double Two-Electron Oxidation of a Molecular Rectangle

Neeladri Das,* Atta M. Arif, and Peter J. Stang*

University of Utah, Department of Chemistry 315 South 1400 East, Room 2020, Salt Lake City, Utah 84112

Monika Sieger, Biprajit Sarkar, and Wolfgang Kaim*

Institut für Anorganische Chemie, Universität Stuttgart, Pfaffenwaldring 55, D-70550 Stuttgart, Germany

Jan Fiedler

J. Heyrovský Institute of Physical Chemistry, Academy of Sciences of the Czech Republic, Dolejškova 3, CZ-18223 Prague, Czech Republic

Received December 23, 2004

Two Pt_4–Fe_2 mixed-metal neutral assemblies, **4** and **5**, incorporating four bis(triethylphosphine)platinum(II) centers, two flexible bridging 1,1′-ferrocenedicarboxylates, and two rigid 2,9-phenanthrenediyl (**4**) or 1,8-anthracenediyl (**5**) bridges, have been synthesized. X-ray characterization of **4** and **5** reveals the formation of discrete and highly symmetrical heterobimetallic neutral species possessing a rhomboidal and rectangular shape, respectively. The rectangular molecules, **5**, could be reversibly oxidized in two two-electron steps, separated by 0.21 V. Spectroelectrochemistry in the UV–vis–NIR region confirms the ferrocene groups as primary oxidation sites; however, the intermediate $\mathbf{5}^{2+}$ is EPR silent even at 4 K due to enhanced EPR relaxation involving the oxidizable 1,8-anthracenediyl linkers.

Introduction

Self-assembly of simple building units into finite, nanoscopic two-dimensional (2D) and three-dimensional (3D) supramolecular structures with well-defined shapes is a prominent field of research in contemporary chemistry.[1] Coordination-driven self-assembly utilizes metal systems as key elements in the generation of molecular ensembles.[1] During the past decade, homometallic discrete assemblies have been the dominant synthetic targets. Much of this construction has been based on the coordinating motif between Pd(II)/Pt(II) acceptor units and nitrogen donor ligands.[1a−c,e,k]

Heterobimetallic polymeric networks[2] are exciting because they have the potential to exhibit interesting physical properties such as electronic coupling between different metal centers. Organometallic compounds, especially ferrocene and its derivatives, have been used as starting materials toward the synthesis of products possessing useful electrochemical, magnetic, and optical properties.[3]

We have recently reported that oxygen−platinum coordination is an effective way of preparing neutral (2D) Pt-

* To whom correspondence should be addressed. E-mail: stang@chem.utah.edu (P.J.S.), kaim@iac.uni-stuttgart.de (W.K.).

(1) (a) Seidel, S. R.; Stang, P. J. *Acc. Chem. Res.* **2002**, *35*, 972. (b) Swiegers, G. F.; Malefetse, T. J. *Coord. Chem. Rev.* **2002**, *225*, 91. (c) Holliday, B. J.; Mirkin, C. A. *Angew. Chem., Int. Ed.* **2001**, *40*, 2022. (d) Cotton, F. A.; Lin, C.; Murillo, C. A. *Acc. Chem. Res.* **2001**, *34*, 759. (e) Fujita, M.; Umemoto, K.; Yoshizawa, M.; Fujita, N.; Kusukawa, T.; Biradha, K. *Chem. Commun.* **2001**, 509. (f) Leininger, S.; Olenyuk, B.; Stang, P. J. *Chem. Rev.* **2000**, *100*, 853. (g) Uller, E.; Demleitner, I.; Bernt, I.; Saalfrank, R. W. Synergistic Effect of Serendipity and Rational Design in Supramolecular Chemistry. In *Structure and Bonding*; Fujita, M., Ed.; Springer: Berlin, 2000; Vol. 96, p 149. (h) Caulder, D. L.; Raymond, K. N. *J. Chem. Soc., Dalton Trans.* **1999**, 1185. (i) Caulder, D. L.; Raymond, K. N. *Acc. Chem. Res.* **1999**, *32*, 975. (j) Baxter, P. N. W.; Lehn, J.-M.; Baum, G.; Fenske, D. *Chem. Eur. J.* **1999**, *5*, 102. (k) Fujita, M. *Chem. Soc. Rev.* **1998**, *27*, 417. (l) Chambron, J.-C.; Dietrich-Buchecker, C.; Sauvage, J.-P. Transition Metals as Assembling and Templating Species. In *Comprehensive Supramolecular Chemistry*; Lehn, J.-M., Chair, E., Atwood, J. L., Davis, J. E. D., MacNicol, D. D., Vogtle, F., Eds.; Pergamon Press: Oxford, 1996; Vol. 9, Chapter 2, p 43. (m) Lehn, J.-M. *Supramolecular Chemistry: concepts and perspectives*; VCH: New York, 1995.

10.1021/ic0481834 CCC: $30.25
Published on Web 07/08/2005

Scheme 1. Self-assembly of Heterobimetallic, Neutral, Pt−Ferrocene-Based Macrocycles

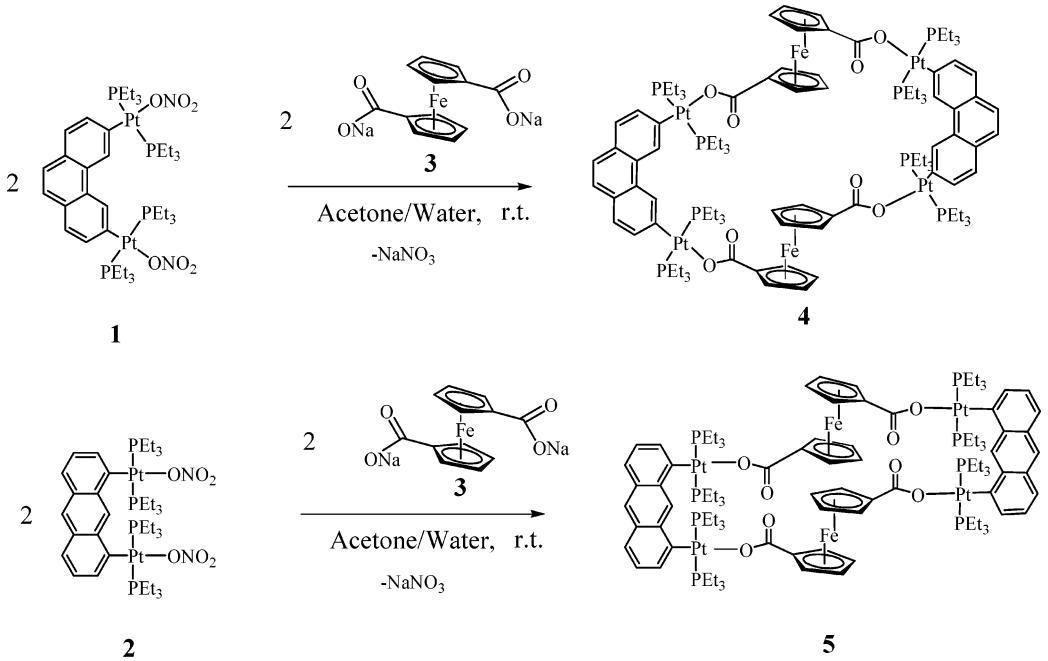

macrocycles.[4] The Pt(II)-based 60° building block from precursor **1**[5a] and the organometallic clip from precursor **2**[5b] were linked with linear and angular dicarboxylate anions to produce rectangles, triangles, and rhomboids.[4a,b] Using this new paradigm, we were interested in incorporating redox active sites in the final macrocycle, replacing the previously used nonfunctional spacers such as terephthalate, fumarate, or muconate.[4] A suitable candidate was 1,1′-ferrocenedicarboxylic acid, **3**. Unlike other aromatic dicarboxylates, **3** is a more flexible linker capable of various geometries under different coordinating modes.[6]

Ferrocene **3** has been used extensively in the construction of heterobimetallic coordination polymers.[3,6] However, only a few examples of finite, neutral, and at the same time heterobimetallic assemblies including **3** and Mo,[7a] Ga,[7b] Re[7c], and Zn[7d] are known to date. We were interested in preparing neutral 2D heterobimetallic macrocycles via coordination-driven self-assembly using our Pt(II) acceptor linkers and ferrocene derivative **3**. Herein, we report the synthesis and characterization of two Pt(II) ferrocene-containing neutral macrocyclic complexes, **4** and **5** (Scheme 1).

Compound **5** contains two different kinds of reversibly oxidizable components, the ferrocene groups and the carbanionic 1,8-anthracenediyl clips. While there is continued interest in the electrochemistry of supramolecular assemblies,[8−10] it may be noted that molecular rectangles with one reducible and one oxidizable group (compounds **6** and **7**, cf. below)[9] or with two kinds of reducible bridges[10] have been reported; however, compound **5** represents a first example with *two very different kinds of oxidizable sides* of such a rectangular arrangement.

(2) (a) Larionova, J.; Kahn, O.; Gohlen, S.; Ouahab, L.; Clerac, R. *J. Am. Chem. Soc*. **1999**, *121*, 3349. (b) Coronado, E.; Galan-Mascaros, J. R.; Gomez-Garcia, C. J.; Ensling, J.; Gutlich, P.; *Chem. Eur. J*. **2000**, *6*, 552. (c) Seiber, R.; Decurtins, S.; Stoeckli-Evans, H.; Wilson, C.; Yufit, D.; Howard, J. A. K.; Capelli, S. C.; Hauser, A. *Chem. Eur. J*. **2000**, *6*, 361. (d) Dong, Y. B.; Smith, M. D.; Loye, H. C. *Angew. Chem., Int. Ed.* **2000**, *39*, 4271. (e) Dong, Y. B.; Smith, M. D.; Loye, H. C. *Inorg. Chem*. **2000**, *39*, 1943. (f) Kamiyama, A.; Noguchi, T.; Kajiwara, T.; Ito, T. *Angew. Chem., Int. Ed.* **2000**, *39*, 3130.

(3) (a) Plenio, H.; Aberle, C.; Al Shihadeh, Y.; Lloris, J. M.; Martinez-Manez, R.; Pardo, T.; Soto, J. *Chem.-Eur. J.* **2001**, *7*, 2848. (b) Jutzi, P.; Lenze, N.; Neumann, B.; Stammler, H. G. *Angew. Chem., Int. Ed.* **2001**, *40*, 1424. (c) Miller, J. S.; Epstein, A. J.; Reiff, W. M. *Acc. Chem. Res.* **1988**, *21*, 114. (d) *Ferrocenes: Homogeneous Catalysis, Organic Synthesis, Materials Science*; Togni, A., Hayashi, T., Eds.; VCH: Weinheim, Germany, 1995. (e) Long, N. J. *Metallocenes: An Introduction to Sandwich Complexes*; Blackwell Science, Inc.: Cambridge, MA, 1998. (f) Bradley, S.; Camm, K. D.; Liu, X. M.; McGowan, P. C.; Mumtaz, R.; Oughton, K. A.; Podesta, T. J.; Thoronton-Pett, M. *Inorg. Chem.* **2002**, *41*, 715 (g) Gibson, V. C.; Long, N. J.; White, A. P. J.; Williams, C. K.; Williams, D. J. *Chem Commun*. **2000**, *23*, 2359. (h) Horikoshi, R.; Mochida, T.; Moriyama, H. *Inorg. Chem.* **2002**, *41*, 3017. (i) Braga, D.; Polito, M.; D'Addario D.; Tagliavini, E.; Proserpio, D. M.; Grepioni, F.; Steed, J. W. *Organometallics* **2003**, *22*, 4532. (j) Chandrasekhar, V.; Nagendran, S.; Bansal, S.; Kozee, M. A.; Powell, D. R. *Angew. Chem., Int. Ed.* **2000**, *39*, 1833.

(4) (a) Das, N.; Mukherjee, P. S.; Arif, A. M.; Stang, P. J. *J. Am. Chem. Soc*. **2003**, *125*, 13950. (b) Mukherjee, P. S.; Das, N.; Kryschenko, Y. K.; Arif, A. M.; Stang, P. J. *J. Am. Chem. Soc*. **2004**, *126*, 2464.

(5) (a) Kryschenko, Y. K.; Seidel, S. R.; Arif, A. M.; Stang, P. J. *J. Am. Chem. Soc*. **2003**, *125*, 5193. (b) Kuehl, C. J.; Huang, S. D.; Stang, P. J. *J. Am. Chem. Soc*. **2001**, *123*, 9634.

(6) (a) Dong, G.; Hong, M.; Chun-ying D.; Feng, L.; Qing-jin M. *J. Chem. Soc., Dalton Trans.* **2002**, 2593. (b) Yang, Y. Y.; Wong, W. T. *Chem. Commun*. **2002**, 2716. (c) Dong, G.; Yu-ting, L.; Chun-ying D.; Hong M.; Qing-jin, M. *Inorg. Chem.* **2003**, *42*, 2519.

(7) (a) Cotton, F. A.; Daniels, L. M.; Lin, C.; Murillo, C. A. *J. Am. Chem. Soc*. **1999**, *121*, 4538. (b) Uhl W.; Spies, T.; Haase, D.; Winter R.; Kaim, W. *Organometallics* **2000**, *19*, 1128. (c) Bera, J. K.; Clerac, R.; Fanwick, P. E.; Walton, R. A. *J. Chem. Soc., Dalton Trans.* **2002**, 2168. (d) Zevaco, T. A.; Gorls, H.; Dinjus, E. *Polyhedron* **1998**, *17*, 613.

(8) Kaifer, A. E.; Gómez-Kaifer, M. *Supramolecular Electrochemistry*; Wiley-VCH: Weinheim, Germany, 1999.

(9) Kaim, W.; Schwederski, B.; Dogan, A.; Fiedler, J.; Kuehl, C. J.; Stang, P. J. *Inorg. Chem*. **2002**, *41*, 4025.

(10) (a) Hartmann, H.; Berger, S.; Winter, R.; Fiedler, J.; Kaim, W. *Inorg. Chem.* **2000**, *39*, 4977. (b) Benkstein, K. D.; Hupp, J. T.; Stern, C. L. *Angew. Chem., Int. Ed*. **2000,** *39*, 2891. (c) Dinolfo, P. H.; Williams, M. E.; Stern, C. L.; Hupp, J. T. *J. Am. Chem. Soc.* **2004**, *126*, 12989.

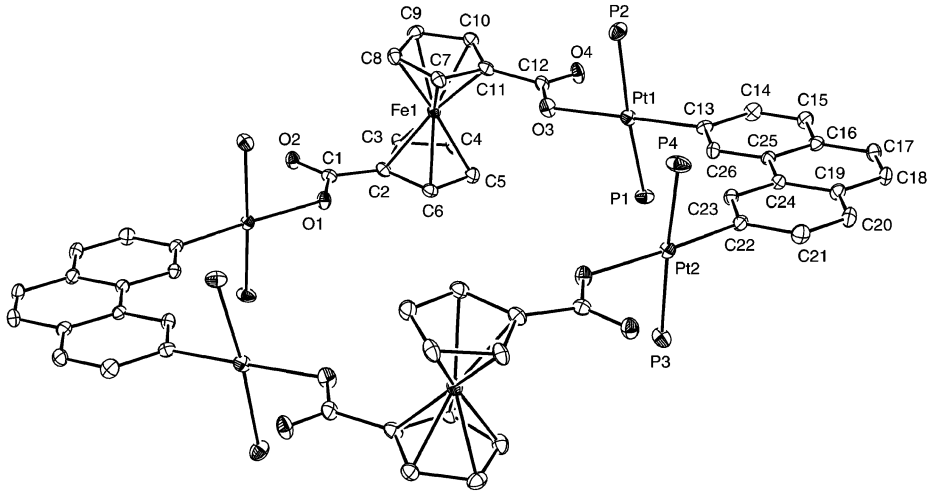

Figure 1. ORTEP diagram of **4**. The ethyl groups attached to the phosphorus atoms and solvent molecules have been omitted for clarity. Thermal ellipsoids are drawn to 30% probability.

Results and Discussion

Addition of an aqueous solution of **3** to an acetone solution of platinum acceptor **1** resulted in gradual precipitation of the neutral rhomboidal macrocycle **4** in 95% isolated yield. $^{31}P\{^1H\}$ NMR analysis of the precipitate indicated the formation of a single highly symmetrical species by the appearance of a sharp singlet with concomitant ^{195}Pt satellites, shifted 2.30 ppm upfield relative to that of **1**. The small change in the position of the phosphorus resonance in comparison to that of the starting material **1** is expected due to the formation of a Pt−OOC coordinate bond replacing a similar $Pt-ONO_2$ coordinate bond in the starting linker. Likewise, the reaction of **2** with **3** yields **5** in 95% isolated yield. The $^{31}P\{^1H\}$ NMR spectrum was similar to that of **4** with a single resonance near 13 ppm. Examination of the ^1H NMR spectra of each product showed that **3** had indeed been successfully incorporated. Two triplets centered near 4.8 and 4.3 ppm were assigned to the protons on the Cp rings in both cases.

Diffraction-quality single crystals of **4** were grown overnight by vapor diffusion of acetone into a $CHCl_3/CH_2Cl_2$ solution of the complex. X-ray crystallography unambiguously established its structure. Figure 1 shows the ORTEP representation of **4**.

The crystallographic data and refinement parameters are given in Table 1. Characteristic bond parameters are shown in Table 2. The coordination mode of the carboxylate groups in **4** is syn-syn[4a] and the torsion angle for the two Cp rings is ca. 156°, as shown in Figure 2. Hence, the ferrocenyl spacer groups adopt an anticlinal eclipsed conformation [Chart 1(c), Supporting Information]. The cavity dimensions of rhomboid **4** are 14 Å × 20 Å (Figure 2). These values are close to previously reported neutral rhomboids.[4b] Highly disordered dichloromethane molecules were present between the rhomboids in the solid state.

The packing nature of adjacent macrocycles produces exterior channels that are also rhomboidal in shape and are occupied by dichloromethane molecules. The Pt−Pt distance between each layer is 11.03 Å, viewed along the *a* axis. This distance is close to that of other cationic and neutral rhomboids reported earlier.[4,11]

Table 1. Crystallographic Data and Refinement Parameters for **4** and **5**

compound	**4**	**5**
formula	$C_{105}H_{162}Cl_{10}Fe_2O_8P_8Pt_4$	$C_{103}H_{158}Cl_6Fe_2O_8P_8Pt_4$
fw	3046.67	2876.81
temp (K)	150(1)	150(1)
λ (Å)	0.71073	0.71073
cryst syst	Triclinic	Monoclinic
space group	$P\bar{1}$	$C2/c$
a (Å)	11.03410(10)	40.0355(12)
b (Å)	16.2572(3)	10.4098(2)
c (Å)	17.7300(3)	30.4252(9)
α (deg)	101.2892(7)	90
β (deg)	96.4838(10)	112.9492(9)
γ (deg)	90.7274(10)	90
V (Å^3)	3097.0(8)	11676.4(5)
Z	1	4
D_{calc} (g/cm^3)	1.634	1.636
μ (mm^{-1})	5.096	5.312
F (000)	1510	5704
reflns collected	22794	22379
unique reflns	13993	13292
max and min trans	0.5571 and 0.2476	0.5451 and 0.2731
R1[a][$1 > 2\sigma(I)$]	0.0417	0.0571
wR2	0.0923	0.1250

[a] $R1 = (F_o - F_c)/F_o$, $wR2 = [(w(F_o^2 - F_c^2)^2)/(F_o^2)^2]^{1/2}$.

Quality single crystals of **5** grew at ambient temperature by vapor diffusion of acetone into a concentrated $CHCl_3/CH_2Cl_2$ solution. X-ray crystallography clearly established that complex **5** has a rectangular shape. Figure 3 shows the ORTEP representation of **5**.

Important crystallographic parameters are given in Table 1. Selected bond parameters are cited in Table 2. Similar to rhomboid **4**, the dicarboxylate in **5** is linked in a syn-syn[4a] fashion. The torsion angle for the two Cp rings is ca. 146°, as shown in Figure 4.

Evidently, the ferrocenyl spacer group also adopts an anticlinal eclipsed conformation [Chart 1(c), Supporting Information] analogous to that in complex **4**. The cavity

(11) (a) Fujita, M.; Aoyagi, M.; Ogura, K. *Inorg. Chim. Acta* **1996**, *246*, 53. (b) Habicher, T.; Nierengarten, J.-F.; Gramlich, V.; Diederich, F. *Angew. Chem., Int. Ed.* **1998**, *37*, 1917. (c) Hartshorn, C. M.; Steel, P. J. *Inorg. Chem.* 1996, *35*, 6902.

Table 2. Selected Bond Lengths (Å) and Angles (deg) for Complexes **4** and **5**

		compound **4**[a]			
Pt(1)−O(3)	2.120(4)	Pt(1)−P(1)	2.319(2)	Pt(1)−P(2)	2.293(2)
Pt(2)−O(1)#1	2.116(4)	Pt(2)−P(3)	2.297(2)	Pt(2)−P(4)	2.298(2)
O(3)−Pt(1)−P(1)	95.24(1)	O(3)−Pt(1)−P(2)	86.23(1)		
P(1)−Pt(1)−P(2)	173.00(9)	O(1)#1−Pt(2)−P(4)	91.81(1)		
O(1)#1−Pt(2)−P(3)	87.84(1)	P(3)−Pt(2)−P(4)	174.29(7)		
		compound **5**[b]			
Pt(1)−O(3)	2.136(6)	Pt(1)−P(1)	2.308(3)	Pt(1)−P(2)	2.287(3)
Pt(2)−O(1)#1	2.139(6)	Pt(2)−P(3)	2.295(3)	Pt(2)−P(4)	2.305(3)
O(3)−Pt(1)−P(1)	89.99(2)	O(3)−Pt(1)−P(2)	88.25(2)		
P(1)−Pt(1)−P(2)	168.42(1)	O(1)#1−Pt(2)−P(4)	91.96(2)		
O(1)#1−Pt(2)−P(3)	87.97(2)	P(3)−Pt(2)−P(4)	171.38(1)		

[a] Symmetry transformations used to generate equivalent atoms: #1 $-x+2, -y, -z$. [b] Symmetry transformations used to generate equivalent atoms: #1 $-x+3/2, -y+3/2, -z+1$.

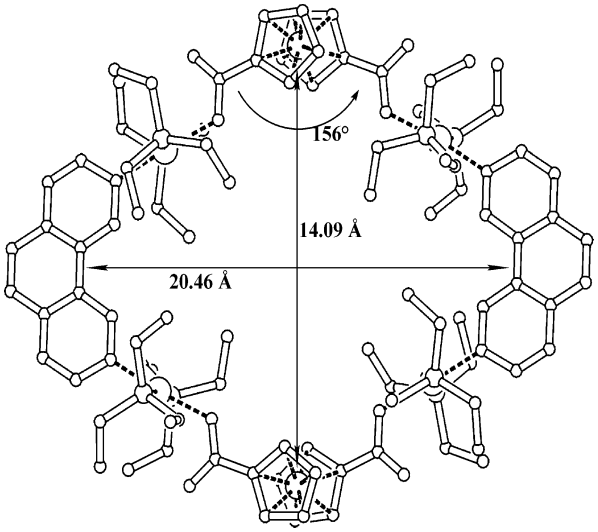

Figure 2. PLATON representation showing the dimensions of **4** and the torsion angle of the ferrocene−dicarboxylato moiety.

dimensions of the rectangular unit **5** are 18 Å × 6 Å (Figure 4). These values are close to previously reported neutral rectangles.[4b] The main molecule is sitting on an inversion center. There are three disordered methylene chloride solvent molecules in the asymmetric unit. The ethyl groups in two triethylphosphine are exhibiting orientation disorder. The Pt−Pt distance between each layer is 10.41 Å, viewed along the *b* axis. This distance is close to that of other cationic and neutral rectangles reported earlier.[4,5b]

Photophysical Properties. Upon formation, complex **5** assumed an intense yellow-orange color. The absorbance in the electronic spectrum of **5** exhibits near-UV transitions which are red-shifted relative to **3** and very slightly blue-shifted relative to **2**. The extinction coefficients of the anthracenediyl and of the ferrocene-based absorbances increase significantly upon formation of **5** (Table 4). These observations are consistent with those previously reported for neutral rectangles.[4b]

Electrochemistry and Spectroelectrochemistry. Cyclic voltammetry of compound **5** in dichloromethane showed two oxidation waves (Figure 5), each corresponding to a double one-electron transfer from the two equivalent ferrocene and anthracene bridges. The cathodic counterpeaks are separated from the corresponding anodic oxidation peaks by about 60 mV. A slightly sharper first peak and the peak separation of 56 mV (Table 3) can be ascribed to partial adsorption on the electrode surface. The scan-rate dependence (i_p vs $v^{1/2}$, Cf. Supporting Information) shows prevailing diffusion control up to 200 mV/s and increasing peak currents at higher scan rates for *both* oxidation peaks, indicating that the adsorption phenomena are associated with the oxidized forms of the complex (cf. the discussion of spectroelectrochemistry). The overall charge consumption of 4 F/mol was verified by coulometry at a potential behind the second oxidation peak. Both the 1,8-anthracenediyl links and the ferrocene units thus appear to behave as noninteracting equivalent redox centers despite the relative short distance between the organometallic sites (Figure 4). The previously investigated rectangular analogues **6** and **7**, which contain the oxidizable

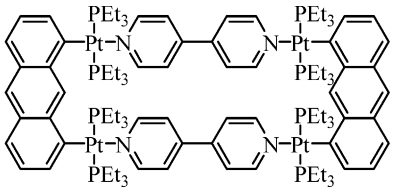

6

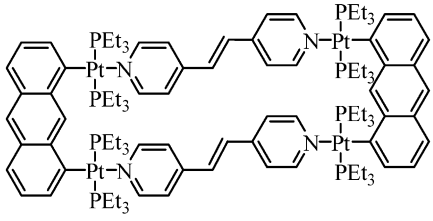

7

anthracenediyl clips as well as reducible *N*-donor π-acceptor bridges, show similar effects;[9] on the other hand, a recently reported dimer of $[PtCl]^+$ with two closely spaced 2,2′-azobispyridine bridges exhibited split reduction waves with an NIR-active ligand-centered mixed valence intermediate.[12]

Although the assignment of the oxidation sequence for the rather close-lying waves was initially ambiguous, it could be anticipated that the less-positive wave of **5** (about 0.4 V less positive in comparison to **6** and **7**) corresponds to the simultaneous oxidation of both ferrocene units and the second

(12) Dogan, A.; Sarkar,B.; Klein, A.; Lissner, F.;. Schleid, Th.; Fiedler, J:; Zalis, S.; Jain, V. K.; Kaim, W. *Inorg. Chem.* **2004**, *43*, 5973.

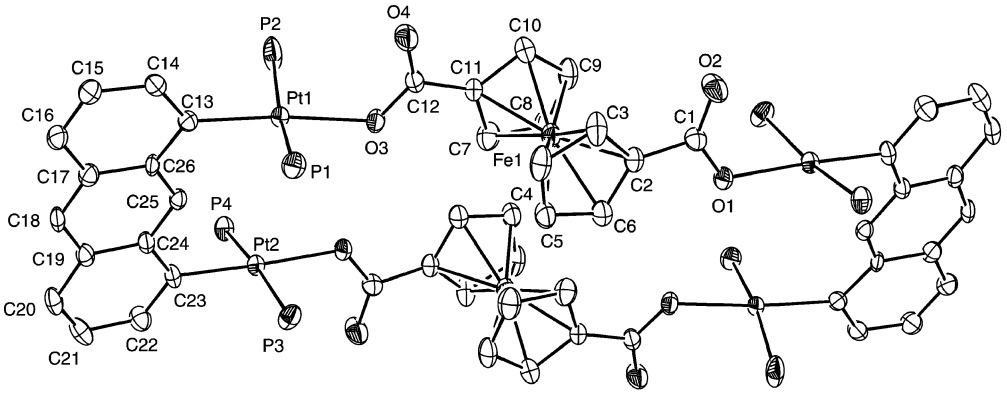

Figure 3. ORTEP diagram of **5**. The ethyl groups attached to the phosphorus atoms have been omitted for clarity. Thermal ellipsoids are drawn to 30% probability.

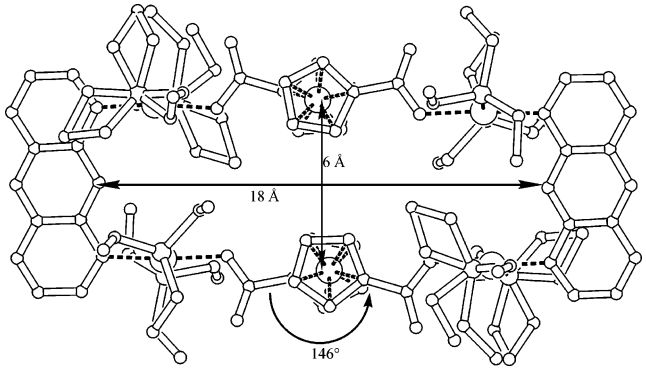

Figure 4. PLATON representation showing the dimensions of **5** and the torsion angle of the ferrocene−dicarboxylato moiety.

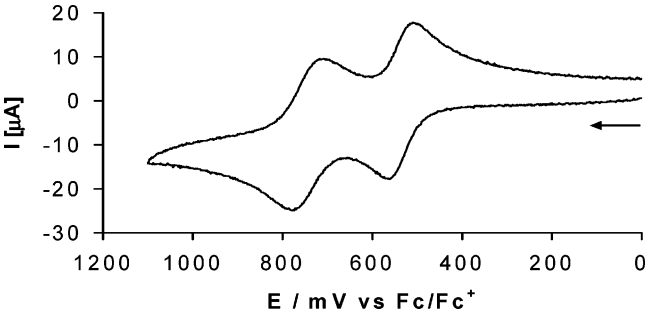

Figure 5. Cyclic voltammetry of a 0.8 mM solution of **5** in CH_2Cl_2/0.1 M Bu_4NPF_6; glassy-carbon electrode, disk diameter 3 mm; scan rate 200 mV/s; 25 °C.

peak to the simultaneous oxidation of the anthracenediyl clips (cf. spectroelectrochemical results below). A slightly lower potential of the clip oxidation in **5** (Table 3) relative to **6** and **7** is expected as a result of less positive charge, even after a preceding ferrocene-based two-electron oxidation step. A further irreversible oxidation process at more positive potential was observed (Table 3), while the reduction of **5** was not detected in the potential range available in CH_2Cl_2—probably another consequence of the lower overall charge.

Despite the seemingly sufficient separation of oxidation waves (Figure 5) resulting in a comproportionation constant for $\mathbf{5}^{2+}$ of $K_c = \exp[nF\Delta E/RT] = 10^{\Delta E/59mV} = 10^{3.6}$ at 298 K ($n = 1$, as the charge transfer to a single site is one-electron), the spectroelectrochemical oxidation of **5** (Figure 6, Table 4) in the first step ($\mathbf{5}/\mathbf{5}^{2+}$) was affected by adsorption

Table 3. Electrochemical Potentials[a] from Cyclic Voltammetry in CH_2Cl_2/0.1 M Bu_4NPF_6

complex	oxidation	reduction
$[Pt_4(PEt_3)_8(\mu\text{-anth})_2\{\mu\text{-}(C_5H_4CO_2)_2Fe\}_2]$ (**5**)	0.12[b] (56)	n.o.[f]
	0.33[b] (66)	
	1.13[c]	
$[Pt_4(PEt_3)_8(\mu\text{-anth})_2(\mu\text{-bp})_2]^{4+}$ (**6**)[d]	0.49[b]	−1.44[b] (69)
	1.17[c]	−2.05[b] (66)
		−2.17[c]
$[Pt_4(PEt_3)_8(\mu\text{-anth})_2(\mu\text{-bpe})_2]^{4+}$ (**7**)[d]	0.55[b]	−1.36[b](67)
	1.28[c]	−1.62[b] (62)
		−1.67[c]
1,1′-(η^5-$C_5H_4CO_2H)_2Fe$ (**3**)[e]	0.46 (75)	

[a] In V vs $[Fe(C_5H_5)_2]^{+/0}$, peak potential differences in mV (in parentheses). [b] Half-wave potentials evaluated from cyclic voltammetry as $E_{1/2} = (E_{pa} + E_{pc})/2$. [c] Peak potentials, E_p, for irreversible processes. [d] In CH_3CN, from ref 9 (reductions localized on bp, bpe ligands). [e] In THF, from ref 17. [f] n.o. = not observed

of the large molecule on the Pt grid electrode and thus did not allow us to completely differentiate between the oxidation steps. The increased adsorption effect in the thin layer cell obviously arises from a relative large area and unpolished surface of the electrode. The change of electrode material in the cyclic voltammetry experiments did not produce a significant difference (see Figure 5 and Supporting Information). The expected weak band at about 600 nm for the ferrocenium chromophore[13] can be observed to be unperturbed only after the very first fractional oxidation (Figure 6, insert, second spectrum); during further oxidation, it is partially obscured by the established[9] intense 1,8-anthracenediyl radical band system around 600 nm (Figure 6, Table 4) due to partial formation of $\mathbf{5}^{4+}$ with one-electron oxidized ferrocene *and* 1,8-anthracenediyl ligands.

Nevertheless, it is evident that the increase of the other anthracenediyl radical bands at 320 and 1200 nm is slow during the beginning of the electrolysis and accelerates only at the end of the first-step oxidation. In contrast, a strong increase is observed during the second-peak oxidation which leads to a 100% ($anth^{\bullet-}$)-containing configuration in $\mathbf{5}^{4+}$. There is a small hypsochromic shift of the near-infrared band during the second-step oxidation which may indicate a slow chemical or conformation change on oxidation; the process

(13) (a) Prins, R. *J. Chem. Soc., Chem. Commun.* **1970**, 280. (b) Sohn, Y. S.; Hendrickson, D. N.; Gray, H. B. *J. Am. Chem. Soc.* **1971**, *93*, 3603.

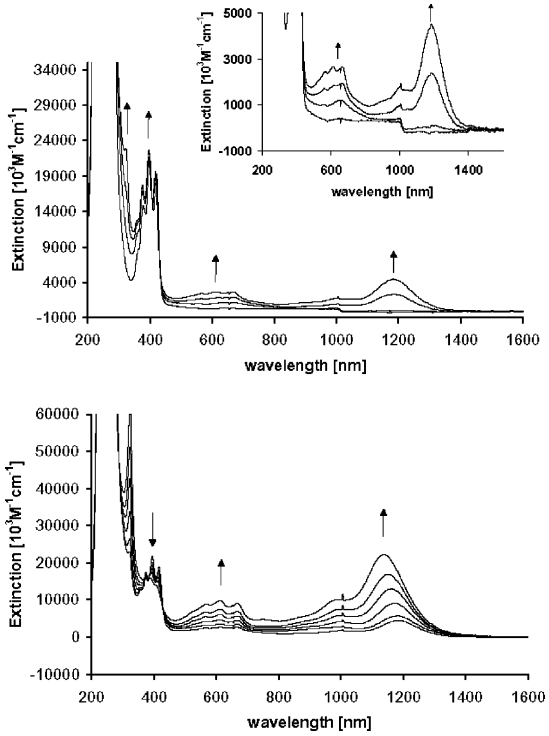

Figure 6. Spectroelectrochemical oxidation of **5** (0.9 mM) in CH_2Cl_2/0.1 M Bu_4NPF_6; spectra during potential scan of the first peak (top) and of the second peak (bottom).

Table 4. Absorption Data Obtained from Spectroelectrochemistry in CH_2Cl_2/0.1 M Bu_4NPF_6

complex	λ_{max}/nm ($\epsilon/10^3$ M^{-1} cm^{-1})
5	227(92.6), 254sh, 267(127.6), 363sh, 379(14.8), 399(21.6), 421(19.1)
$\mathbf{5}^{2+}$	226(86.0), 254sh, 268(130.8), 322(22.9),[a] 359sh, 375(17.5), 396(21.7), 417(18.9), 530sh,[a] 566(2.45),[a] 614(2.65),[a] 665(2.65),[a] 1010(1.71)sh,[a] 1185(4.49)[a]
$\mathbf{5}^{4+}$	226(88.3), 266(110.4), 324(61.8), 372(15.8), 389(15.8), 409(13.8)sh, 529(7.04)sh, 566(8.84), 612(9.83), 668(9.03), 990(10.0)sh, 1137(22.1)

[a] Bands due to partial presence of $\mathbf{5}^{4+}$ (see text).

is reversible since the band maximum is shifted back during spectroelectrochemical re-reduction which leads back to the original neutral compound via the half-oxidized intermediate. An alternative explanation invokes the possible coexistence with a complex form involving oxidized anthracenediyl radicals and non-oxidized ferrocene sites which would show the slightly longer wavelength maximum during the early stages of the electrolysis.

In a simplified view, the oxidation intermediate $\mathbf{5}^{2+}$ exists in equilibrium with the forms **5** and $\mathbf{5}^{4+}$ in a ratio given by the comproportionation constant, K_c. Considering the apparent independence of the redox centers in the actual situation, a statistical distribution of more forms can be expected[14] which may be formulated as follows (R_f/O_f and R_a/O_a stand for reduced/oxidized forms of ferrocene and anthracene centers, respectively):

$R_fR_fR_aR_a$, $O_fR_fR_aR_a$, $R_fR_fO_aR_a$, $O_fO_fR_aR_a$, $O_fR_fO_aR_a$, $R_fR_fO_aO_a$, $O_fO_fO_aR_a$, $O_fR_fO_aO_a$, $O_fO_fO_aO_a$

Supposing sufficiently separated ferrocene- and anthracene-centered redox steps and the presence of only the major, thermodynamically favored species, the formal potentials associated with successive oxidation states can be formulated[14a] according to $E_j^f = E^\circ - (RT/F)\ln[j/(n-j+1)]$ (number of oxidation states $n = 2$; number of reduced sites $j = 1, 2$) as:

(first oxidation peak)

$$E^f(R_fR_fR_aR_a/O_fR_fR_aR_a) \approx E_{1/2}{}^1 - 17.8\ \text{mV},$$

$$E^f(O_fR_fR_aR_a/(O_fO_fR_aR_a) \approx E_{1/2}{}^1 + 17.8\ \text{mV}$$

(second oxidation peak)

$$E^f(O_fO_fR_aR_a/O_fO_fO_aR_a) \approx E_{1/2}{}^2 - 17.8\ \text{mV},$$

$$E^f(O_fO_fO_aR_a/O_fO_fO_aO_a) \approx E_{1/2}{}^2 + 17.8\ \text{mV} \quad (T = 298\ \text{K})$$

The potential difference of 35.6 mV (17.8 + 17.8 V) results in a cyclic voltammogram with the shape of that for a single-electron-transfer process[14b] and increased current intensity due to the overall two-electron reaction. However, in the actual case of relatively close potentials for the oxidations of two different centers and possible adsorption effects during electrolysis in the OTTLE cell, a reasonable probability may exist also for the population of the other states listed above. Therefore, the forms involving oxidized anthracene and non-oxidized ferrocene sites can participate and influence the spectral changes during intermediate stages of the electrolysis. In a less-polar solvent, the expected increasing adsorption of positively charged oxidation products can facilitate charge transfer from the anthracene units and thus effectively decrease the potential difference between the oxidation steps under the conditions of a thin-layer solution and a large area of the electrode.

EPR spectroscopic monitoring during the oxidation of **5** in CH_2Cl_2/0.1 M Bu_4NPF_6 did not show any detectable signals over the entire *g* range, even at 4 K. This EPR silence despite spectroelectrochemically detectable ferrocenium and anthracenediyl radicals points to very rapid EPR relaxation due to the close-lying states $[(\text{ferrocenium})_2(\text{anth}^{2-})_2]^{2+}$ and $[(\text{ferrocene})_2(\text{anth}^{\bullet-})_2]^{2+}$. In other words, the oxidizable organic clips provide an additional pathway for rapid EPR relaxation, broadening the generally difficult-to-detect[15] ferrocenium EPR signals beyond detection even at 4 K and thus providing at least indirect evidence for the interaction between the organic and the organometallic oxidation sites.

In conclusion, two new Pt_4-Fe_2 mixed-metal assemblies have been synthesized. These ensembles are important not only for their aesthetic appeal but also for their intramolecular electron-transfer effects. Compound **5**, a first example with two very different kinds of reversibly *oxidizable* sides of a

(14) (a) Flanagan, J. B.; Margel, S.; Bard, A. J.; Anson, F. C. *J. Am. Chem. Soc.* **1978**, *100*, 4248. (b) Ammar, F.; Savéant, J. M. *J. Electroanal. Chem.* **1973**, *47*, 215.

(15) (a) Elschenbroich, C.; Bilger, E.; Ernst, R. D.; Wilson, D. R.; Kralik, M. S. *Organometallics* **1985**, *4*, 2068. (b) Sixt, T.; Fiedler, J.; Kaim, W. *Inorg. Chem. Commun.* **2000**, *3*, 80.

molecular rectangle could be reversibly oxidized in two two-electron steps, separated by 0.21 V. Spectroelectrochemistry confirmed the ferrocene groups as primary oxidation sites; however, the intermediate $\mathbf{5}^{2+}$ was found to be EPR silent even at 4 K due to rapid EPR relaxation. Other macromolecules using different Pt-acceptor ligands in conjunction with **3** are being synthesized, and their redox properties are currently under investigation.

Experimental Section

Methods and Materials. 1,1′-Ferrocenedicarboxylic acid, **3**, was purchased from Alfa-Aesar and used as received. The disodium salt of **3** was prepared by neutralizing it with $NaHCO_3$ in aqueous medium. 2,9-Bis[*trans*-$Pt(PEt_3)_2NO_3$]phenanthrene, **1**,[5a] and 1,8-bis[*trans*-$Pt(PEt_3)_2NO_3$]anthracene, **2**,[5b] were prepared according to known procedures. Deuterated solvents were purchased from CIL. All NMR spectra were recorded on Varian Unity 300 or Varian XL-300 spectrometers. ^{1}H chemical shifts are reported relative to the residual protons of deuterated dichloromethane ($\delta = 5.32$ ppm). ^{31}P{H} chemical shifts are reported relative to an external, unlocked sample of H_3PO_4 ($\delta = 0.0$ ppm). Elemental analyses were performed by Atlantic Microlab, Norcross, GA. UV−vis spectra were recorder on a Hewlett-Packard 8452A spectrophotometer. Cyclic voltammetry was carried out in CH_2Cl_2 (HPLC grade)/0.1 M Bu_4NPF_6 solutions using a three-electrode configuration (glassy carbon or Pt working electrode, Pt counter electrode, Ag/AgCl reference) and a PAR 273 potentiostat and function generator. IR compensation (positive feedback) was applied routinely. The ferrocene/ferrocenium (Fc/Fc^+) couple served as internal reference. Controlled potential coulometry was performed in a bulk electrolysis cell with a platinum grid working electrode, Ag/AgCl reference electrode, and platinum counter electrode positioned in a sidearm of the cell separated from the electrolyzed solution by sintered glass. Spectroelectrochemistry was performed using an optically transparent thin-layer electrode (OTTLE) cell;[16] the UV−vis−NIR absorption spectra were recorded on a J&M TIDAS spectrophotometer. A two-electrode capillary served to generate intermediates for X-band EPR studies. EPR measurements were performed with a Bruker System ESP 300 equipped with an Oxford Instruments cryostat.

General Procedure for the Preparation of 4 and 5. To a 3 mL acetone solution containing 11.62 mg (0.01 mmol) of organoplatinum reagents **1** or **2**, an aqueous solution (3 mL) of disodium salt **3** (0.01 mmol) was added dropwise with stirring (15 min) during which time a precipitate formed. This was centrifuged, washed several times with water and then acetone, and finally dried in an oven at 60 °C. The products **4** and **5** were redissolved in CD_2Cl_2 for NMR analysis.

Cyclobis[(2,9-bis[*trans*-$Pt(PEt_3)_2$]phenanthrene)(1,1′-ferrocenedicarboxylate)] 4. Yield 95.0%. ^{31}P{1H} NMR (CD_2Cl_2, 121.4 MHz): δ 16.9 (s, $^1J_{PPt} = 2899.7$ Hz). ^{1}H NMR (CD_2Cl_2, 300 MHz): 8.72 (s, 4H, H_1 of **1**), 7.70 (d, 4H, $^3J_{H4-H3} = 8.15$ Hz, H_3 of **1**), 7.45 (s, 4 H, H_5 of **1**), 7.39 (d, 6H, $^3J_{H4-H3} = 8.06$ Hz, H_4), 4.69 (t, 8H, H_2,H_5 of **3**), 4.30 (t, 8H, H_3,H_4 of **3**), 1.70 (m, 48H, PCH_2CH_3 of **1**), 1.20 (m, 72H, PCH_2CH_3 of **1**). Anal. Calcd for $C_{100}H_{152}O_8P_8Pt_4Fe_2$: C, 45.81 H, 5.84% Found: C, 45.64 H, 5.91%.

Cyclobis[(1,8-bis[*trans*-$Pt(PEt_3)_2$]anthracene)(1,1′-ferrocenedicarboxylate)] 5. Yield 95.0% ^{31}P{1H} NMR (CD_2Cl_2, 121.4 MHz): δ 13.4 (s, $^1J_{PPt} = 2876.8$ Hz). ^{1}H NMR (CD_2Cl_2, 300 MHz): δ 9.89 (s, 2H, H_9 of **2**), 8.18 (s, 2H, H_{10} of **2**), 7.65 (d, 4H, $^3J_{HH} = 6.7$ Hz, $H_{4,5}$ of **2**), 7.55 (d, 4H, $^3J_{HH} = 8.38$ Hz, $H_{2,7}$ of **2**), 7.00 (t, 4H, $H_{3,6}$ of **2**), 4.94 (t, 8H, H_2,H_5 of **3**), 4.36 (t, 8H, H_3,H_4 of **3**), 1.70 (m, 48H, PCH_2CH_3 of **2**), 1.05 (m, 72H, PCH_2CH_3 of **2**) Yield: 94.7%. Anal. Calcd for $C_{100}H_{152}O_8P_8Pt_4Fe_2 \cdot 2H_2O$: C, 45.19 H, 5.92% Found: C, 45.22 H, 5.97%.

Acknowledgment. Financial support by NSF (CHE-0306720) at Utah, DFG (Germany), and GACR (Czech Republic) is gratefully acknowledged.

Supporting Information Available: ^{31}P and ^{1}H NMR spectra of **3a** and **3b** (four figures) (PDF), UV−vis absorption spectra of **2**, **3**, and **5**, cyclic voltammogram, peak current/rate correlation (two figures), a chart showing conformations of ferrocenyl rings (one figure), and X-ray crystallographic files (in CIF format) of **4** and **5**. This material is available free of charge via the Internet at http://pubs.acs.org.

IC0481834

(16) Krejcik, M.; Danek, M.; Hartl. F. *J. Electroanal. Chem. Interfacial Electrochem.* **1981**, *317*, 179.
(17) Frosh, W.; Back, S.; Lang, H. *Organometallics* **1999**, *18*, 5725.